International Journal of Nanomedicine

Dovepress
open access to scientific and medical research

Open Access Full Text Article

ORIGINAL RESEARCH

TAT-Modified Gold Nanoparticles Enhance the Antitumor Activity of PAD4 Inhibitors

This article was published in the following Dove Press journal:
International Journal of Nanomedicine

Songlin Song[1,2]
Lin Gui[1,2]
Qiqi Feng[1,2]
Ayijiang Taledaohan[1,2]
Yuanming Li[3]
Wei Wang[4]
Yanming Wang[5]
Yuji Wang[1,2]

[1]School of Pharmaceutical Sciences of Capital Medical University, Beijing 100069, People's Republic of China; [2]Beijing Area Major Laboratory of Peptide and Small Molecular Drugs, Engineering Research Center of Endogenous Prophylactic of Ministry of Education of China, Beijing 100069, People's Republic of China; [3]Minimally Invasive Tumor Therapies Center, Beijing Hospital, National Center of Gerontology; Institute of Geriatric Medicine, Chinese Academy of Medical Sciences, Beijing, 100730, People's Republic of China; [4]Department of Chemistry, University of Bergen, Bergen, Norway; [5]School of Life Sciences, Henan University, Kaifeng 475004, People's Republic of China

Correspondence: Yuji Wang
School of Pharmaceutical Sciences of Capital Medical University, Beijing 100069, People's Republic of China
Tel +86 10 83950236
Email wangyuji@ccmu.edu.cn

Purpose: Histone citrullination by peptidylarginine deiminases 4 (PAD4) regulates the gene expression of tumor suppressor. In our previously study, YW3-56 (356) was developed as a potent PAD4 inhibitor for cancer therapy with novel function in the autophagy pathway. To enhance the antitumor activity, the PAD4 inhibitor 356 was modified by the well-established cationic penetrating peptide RKKRRQRRR (peptide TAT) and gold nanoparticles to obtain 356-TAT-AuNPs which could enhance the permeability of chemical drug in solid tumor.

Methods: 356-TAT-AuNPs were prepared, and their morphology were characterized. The antitumor activity of 356-TAT-AuNPs was evaluated in vitro and in vivo.

Results: 356-TAT-AuNPs exhibited higher anticancer activity against HCT-116, MCF-7 and A549 cells than 356 and 356-AuNPs. Compared with 356 and 356-AuNPs, 356-TAT-AuNPs entered the cytoplasm and nuclear, exhibited stronger anticancer activity by increasing apoptosis, inducing autophagy and inhibiting of histone H3 citrullination, and in HCT-116 xenograft mouse model, 356-TAT-AuNPs could improve the antitumor activity.

Conclusion: The modified AuNPs with peptide TAT as drug delivery system are potent in delaying tumor growth and could be a powerful vehicle for profitable anticancer drug development. We believe that peptide TAT modification strategy may provide a simple and valuable method for improving antitumor activity of PAD4 inhibitors for clinical use.

Keywords: Au nanoparticle, transmembrane peptide, PAD4 inhibitor, antitumor

Introduction

PADs are a family of calcium dependent enzymes that could post-translationally convert Arginine (Arg) residues with positive charges to neutrally charged Citrulline.[1] PAD-mediated citrullination could alter the tertiary structure of target peptide and/or the protein-protein interactions, thereby modifying various cellular processes.[2] Recently, protein citrullination (Cit) has received increased attention due to its functions in various human cancers as well as its implication in the pathogenesis of different inflammatory conditions.[3] This type of protein or peptide modification was first explored in autoimmune disorder, such as rheumatoid arthritis.[4] Among this Cit process catalyzed by the PADs family, the well-known histone Cit provides the important mechanism for neutrophil extracellular traps (NETs) in the peripheral blood.[5] Further explorations revealed that Cit of proteins or peptides is also involved in carcinogenesis process. Citrullinated proteins or peptides disturbed the structure stability, and induced DNA damages. More and more studies show that citrullinated proteins or peptides can be applied as promoting targets for diagnosis or treatment of cancer.[6] The PAD4 inhibitor, YW3-56 (356), could effectively inhibit cancer growth

in sarcoma S-180 bearing mouse model,[7] but water solubility of free 356 is rather poor.

In this study, we designed Au nanoparticles (Au-NPs) as drug delivery systems for compound 356 to increase the antitumor activity on gastrointestinal cancer cells and improve its solubility (as shown in Figure 1). Recently, functionalized Au-NPs system represents highly appealing and promising options for drug controlled releasing and drug delivery, owing to the special dimensions and tunable functionalities of Au-NPs' surface, especially.[8–10] Peptide TAT, derived from HIV and discovered as the first cell-penetrating peptide (CPP), has been widely designed to decorate drug delivery systems and bio-functional molecules.[11–13] Here we report the design of gold nanoparticles modified by TAT to improve the transmission to the nucleus and kill cancer cells.

Materials and Methods

Materials

Chemistry. General Methods. Silica gel thin-layer chromatography (TLC) separations were performed on GF-254 plates (Qingdao Haiyang Chemical, China). All organic solvents and reagents were analytically pure with no further purification. All starting materials in the synthesis were commercially available. ^{1}H NMR and ^{13}C NMR spectra were performed and recorded on AVANCE 300 spectrometers (Bruker Company, Germany) using DMSO-*d6* as the solvent and TMS as the internal standard.

Gold chloride trihydrate and Dimethyl sulfoxide were purchased from Aladdin Biochemical Technology (Shanghai, China). PI detection kits were purchased from Solarbio Science &Technology (Beijing, China). Phalloidin FITC Reagent, Anti-Histone H3 citrulline R2 antibody, IgG H&L (Alexa Fluor® 568), PADI4 Rabbit Polyclonal antibody, LC3 antibody, and anti-β-actin primary antibody were provided from Abcam (USA).

Preparation of compound 356: According to the literature,[7] compound 356 was synthesized (Figure S3), seperated and purified by flash chromatography (200–400 mesh silica gel; 5% MeOH/DCM as eluent) to give compound 356 as pale yellow solid. Yield: 47 mg (24% in 5 steps). Compound 356 was further purified using a Waters HPLC system with a reverse phase C18 column (XBridge Peptide BEH C18 OBD 5 μm, eluted by 70%ACN/30%H_2O with 0.1%TFA). ^{1}H NMR (300 MHz, DMSO-*d6*, δ): 10.25 (s, 1H, H^+), 9.61 (s, 1H, =NH), 9.21 (s, 1H, NH), 8.82 (d, J = 9 Hz, 1H; CONH), 8.67 (t, J = 6 Hz, 1H; CONH), 8.25 (s, 1H; Ar H), 7.94 (d, J = 6 Hz, 1H; Ar H), 7.85 (d, J = 6 Hz, 1H;

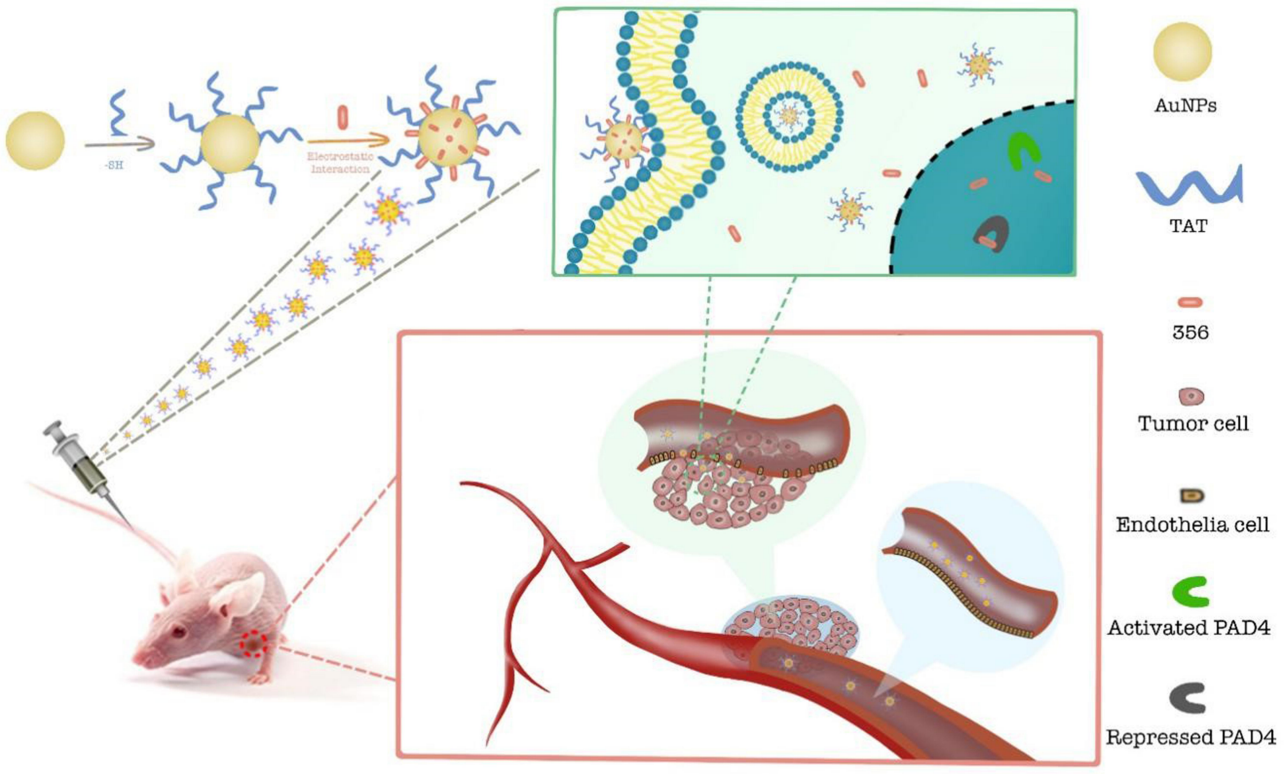

Figure 1 Schematic representation of the 356-TAT-AuNPs formation and delivery system.

Ar H), 7.78 (d, J = 6 Hz, 2H; Ar H), 7.60–7.39 (m, 4H; Ar H), 7.33–7.22 (m, 4H; Ar H), 4.57 (m, 1H; CH), 4.44 (s, 2H; CH_2Cl), 4.31 (d, J = 3 Hz, 2H; $CH_2C_6H_5$), 3.35 (s, 6H; $C(CH_3)_2$), 3.32 (m, 2H; NCH_2), 1.88 (m, 2H; CH_2), 1.66 (m, 2H; CH_2); MS $C_{27}H_{32}ClN_5O_2$ $[M+H]^+$: 494.4. And the spectra were supplied and described in detail in Figure S4–S6 of the Supporting Information.

Preparation of 356-TAT-AuNPs: Au-NPs (17 nm) was prepared by the classical sodium citrate reduction method of HAuCl4 in aqueous phase. The aqueous solution (100 mL, 0.23 mM) of tetrachloroacid trihydrate is heated and refluxed and stirred. When it is boiling, sodium citrate aqueous solution (1%, 5 mL) is quickly added, mixed and stirred for 10 mins, and cooled to room temperature (rt). The product whose color changes to bright red is colloidal solution of gold nanoparticles. Then in order to obtain 356-AuNPs, add the fresh 356 solution (1.5 mL, 0.2 mg/mL, DMSO) to the above prepared colloidal solution of gold nanoparticles, stirring for 3 hours at rt to obtain 356-AuNPs; in order to prepare 356-TAT-AuNPs, TAT solution (20 μL, 0.1 mm, H_2O) was added to the freshly prepared 100 mL solution of gold nanoparticles, stirring for 1 min, and then 1.5 mL 356 solution (0.2 mg/mL, DMSO) was added and stirred at rt for 3 hours to obtain 356-TAT-AuNPs. The prepared sample solutions were sealed overnight in 4 °C, and then the raw materials were removed by centrifugation (8000 rpm, 10 mins), washed and purified with ultrapure water. The precipitates were redistributed in 5 mL of the mixture (DMSO and water, 0.5:99.5).

Nanoparticle Formation and Concentration Determination

The formation of AuNPs in ultrapure water was measured and recorded by UV-vis spectroscopy on a UV-2550 spectrometer (Shimadzu, Kyoto, Japan) ranged from 200 to 800 nm). A series of concentrations (2.0, 5.0, 10.0, 15.0, 20.0, 25.0 and 30.0 μg/mL) of compound 356 were detected by UV-Vis. The absorbance value of compound 356 was set as the y axis in the standard curve, while the concentration of compound 356 was set as the x axis. By using the weighted least-square method, linear regression analysis was then performed. The concentration of 356 in AuNPs was also measured by UV-vis.

Nanoparticle Characterization

The morphology and characterization of the AuNPs were measured by transmission electron microscopy (JEOL, 2100, Japan). The average size and zeta potential of Nanoparticles were detected by a Zetasizer Nano instrument (Malvern, UK). Before dynamic light scattering (DLS) characterization, the AuNPs were diluted in H_2O to 1 mg/mL, the AuNPs in ultrapure water was passed through 0.45 μm polyvinylidene fluoride membrane. The sample was loaded into quartz microcuvette. For each nanoparticle system, data obtained from three detections were averaged to calculate the mean zeta potential and size.

Cell Culture and Cell Viability

Human HCT-116 cells (colorectal carcinoma), human MCF-7 cells (breast cancer) and human A549 cell lines (non-small-cell lung carcinoma) were obtained from American Type Culture Collection (ATCC). HCT-116 and A549 cells were maintained in RPMI 1640 Medium (Gibco by Life Technologies) with 10% fetal bovine serum (FBS). MCF-7 cells were maintained in DMEM (Gibco by Life Technologies) with 10% FBS.

Cell viability treated with different samples was detected by MTT assays. Briefly, 3×10^3 HCT-116, MCF-7 and A549 cells were plated in 96-well plates. After 6 h, the medium was removed and the fresh culture medium containing designed concentrations of AuNPs, 356, 356-AuNPs and 356-TAT-AuNPs. After another 24 h, 25 μL of 5 mg/mL MTT solution was added to the 96-well plate, and the cells were cultured for another 4 h. 100 μL of DMSO was then added to dissolve the purple formazan crystals, and the OD value (492 nm) was detected with a microplate reader (MiniMax 300 Imaging Cytometer, Molecular Devices, USA).

Laser Confocal Microscopy Analysis

The cellular internalization and distributions were observed by confocal microscopy: HCT-116 cells were cultured for 24 h until total adhered on glass-bottom dishes. The cells were then incubated with 356, 356-AuNPs and 356-TAT-AuNPs dissolved in media (Maintain 356 concentration of 5 μM in RPMI 1640 medium) at 37°C for 12 h. Washed with cold PBS three times, the cells were treated with FITC Phalloidin (100 nM) and PI (20 μg/mL) to stain the nucleus and cytoskeleton. Then the cells were characterized immediately and analyzed using a laser scanning confocal microscope (Leica, TCS SP8, Germany). The excitation wavelength and detection wavelength of 356, FITC Phalloidin and PI were 403 and 462 nm, 488 and 530 nm, 535 and 618 nm, respectively.

In vitro Immunofluorescent Staining

Confocal microscopy was used to investigate the effects on Histone H3 Citrullination. Briefly, HCT-116 cells were cultured for 24 h until total adhered on glass-bottom dishes. Then 356, 356-AuNPs and 356-TAT-AuNPs dissolved in media (Maintain 356 concentration of 5 μM in RPMI 1640 medium) were added into the cells and incubated at 37°C for 12 h. Washed with cold PBS three times, 0.1% Triton x-100 was then added to increase the cell permeability; 5% goat serum was added and blocked at rt for 2 h. After washing with PBS, Rabbit Anti-Histone H3 antibody was added and treated at 4 °C for 15 h. After washing thrice with PBS, goat anti-rabbit IgG H&L (Alexa Fluor® 568) was added, and it was treated in a dark box at rt for 1 h. After PBS washing, FITC was added to treated for 45 min. The excitation and emission wavelengths of 356, FITC and Alexa Fluor 568 were 403/462 nm, 488/530 nm, and 578/603 nm, respectively. And the confocal fluorescence images were obtained via confocal laser scanning microscope (CLSM, TCS SP8 STED, Germany).

Apoptosis

Propidium iodide (PI) and Annexin V-FITC stainings were used to characterize the apoptosis of HCT-116 cells treated with 5 μM of 356, 356-AuNPs and 356-TAT-AuNPs diluted in culture medium for another 12 h and 24 h. Control groups were cultured in medium (with 10% FBS). The cells were resuspended in 500 μL of binding buffer (0.14 M NaCl and 2.5 mM $CaCl_2$, 10 nM HEPES, pH 7.5) containing 5 μL of PI and 5 μL of Annexin V-FITC for 30 min at rt in the dark, and then the fluorescence intensity was measured on a flow cytometer (Becton Dickinson FACS Calibur, USA).

Subcellular Ultrastructure and Localization by TEM

The TEM analysis was used to investigate the intracellular localization of 356-TAT-AuNPs inside the HCT-116 cells. The cells were seeded in 24-well plates with plastic cover slips at a density of 1×10^6 cells/well and cultured. After 24 h, the cells were exposed to 356 (5 μM), 356-AuNPs (5 μM), 356-TAT-AuNPs (5 μM) for further 24 h. Then cells were washed three times with PBS, and fixed by 2.5% glutaraldehyde in 100 mM sodium cacodylate buffer for 4 h at 4°C. Then HCT-116 cells were post-fixed in 1% OsO_4 aqueous solution and embedded into epoxy resin later. Thin sections (50~70 nm) were harvested. The ultrastructure were characterized by TEM (JEOL, 2100, Japan).

Cell Uptake by Inductively Coupled Plasma Optical Emission Spectrometer (ICP-OES)

To measure the intracellular uptake of the AuNPs, 356-AuNPs and 356-TAT-AuNPs in HCT-116 cells, cells were grown in 24-well culture plates (5×10^4 cells in 1 mL of the medium per well). After incubation for 24 h at 37°C, the cells were incubated with AuNPs, 356-AuNPs and 356-TAT-AuNPs (Maintain 356 concentration of 5 μM in RPMI 1640 medium) for 4 hand 24 h. After washing three times by PBS, AuNPs were digested in 1 mL of aqua regia solution. Then each sample solution volume was made up to 10 mL in a volumetric flask with distilled water, and the content of Au was measured by ICP-OES.

Western Blotting

Incubated with 5 μM AuNPs, 356, 356-AuNPs and 356-TAT-AuNPs for 8 h, the HCT-116 cells were harvested on ice and lysed. After centrifugation the precipitates were collected, and by using the kit (bicinchoninic acid-protein assay), the total concentration of protein was detected. A total of 20 μg of protein were purified by 10% sodium dodecyl sulphate-polyacrylamide (SDS-PAA) gel and then the protein was transferred to nitrocellulose membranes (Millipore, USA). Followed by blocking with 5% nonfat milk, the membranes were incubated with a rabbit anti-PADI4 Rabbit Polyclonal antibody (dilution 1:1000), rabbit anti-LC3 antibody (dilution 1:1000), or a mouse anti-β-actin monoclonal antibody (dilution 1:2000). The membranes were then incubated with the goat anti-mouse or goat anti-rabbit horseradish peroxidase (HRP) secondary antibody (Sigma, USA). And the protein complex was measured using the enhanced chemiluminescence reagent (Millipore, USA). β-actin was the internal control.

The Therapeutic Efficacy in vivo

The old male BALB/c nude mice (3 to 5-week) were supplied by Charles River Laboratories, and all experimental protocols and procedures were approved by the Institutional Animal Care and Use Committee of Capital Medical University (the Ethics Number AEEI-2018-174). Laboratory animal welfare (PR China National Standard

GB/T 35,892–2018) was given in animal studies. HCT-116 cells of 2×10^6 prepared from 4 tumor bearing mice were xenografted subcutaneously at right flank of the mice. Tumor diameters were detected every other day by a Vernier caliper. The mice were randomly divided into 4 groups (normal saline (NS), AuNPs, 356 and 356-TAT-AuNPs) and treated by drugs when the average volume of tumor reached ~100 mm^3. 356 and 356-TAT-AuNPs were administered (i.p.) twice per week for 6 times altogether. And the samples were prepared and redistributed in the mixture of DMSO and water (0.5:99.5, 5 mL) as same as above in the section of Preparation of 356-TAT-AuNPs. The mice body weights were weighed every other day. Tumor volume (V) was then calculated by the following formula: $V = a^2b/2$ (where a and b represent the shortest and the longest diameter, respectively of the tumor).

Statistical Analysis

All the experiments and bioassays in this study were conducted at least 3 times. Quantitative data were expressed as the mean ± standard deviation. Statistical differences were represented using the GraphPad Prism 7.0 (GraphPad Software, CA). Comparisons between the control and treated groups were performed by One-way and the two-way ANOVA. A *p* value of less than 0.05 was recognized as statistically significant.

Results

Synthesis of Free 356-Loaded Au Nanoparticles 356-AuNPs and 356-TAT-AuNPs

The UV-vis spectra profile of 356-AuNPs and 356-TAT-AuNPs was characterized (Figure S1A). It was determined that compound 356 had a A_{max} (maximum absorption wavelength) of 328 nm at different concentrations. Therefore, A_{max} (328 nm) was set as the wavelength for compound 356's concentration detection. The regression equation was calculated to be y = 0.0326x - 0.0382, with R^2 = 0.9995 (Figure S1B). The absorption spectrum of AuNPs is measured in water, and the absorption peak is at 520 nm. Upon being loaded with 356 and TAT on AuNPs, the large absorption band in 356-AuNPs and 356-TAT-AuNPs shifted from 520 to 560 nm. 356-AuNPs and 356-TAT-AuNPs are negatively charged with mean surface charge of −28.70 ± 4.03 mV and −15.15 ± 0.12 mV, respectively (Table S1).

Au nanoparticles (AuNPs) with a diameter of 16.45 ± 0.82 nm (Figure 2A) were prepared by the classical sodium citrate reduction method of $HAuCl_4$ and characterized at neutral pH by transmission electron microscopy (TEM).[14] 356-AuNPs were prepared by adding a fresh free 356 solution to the above colloidal system. The 356-AuNPs exhibit a relatively narrow size distribution and the average size is 16.60 ± 1.31 nm based on the TEM image (Figure 2B). To

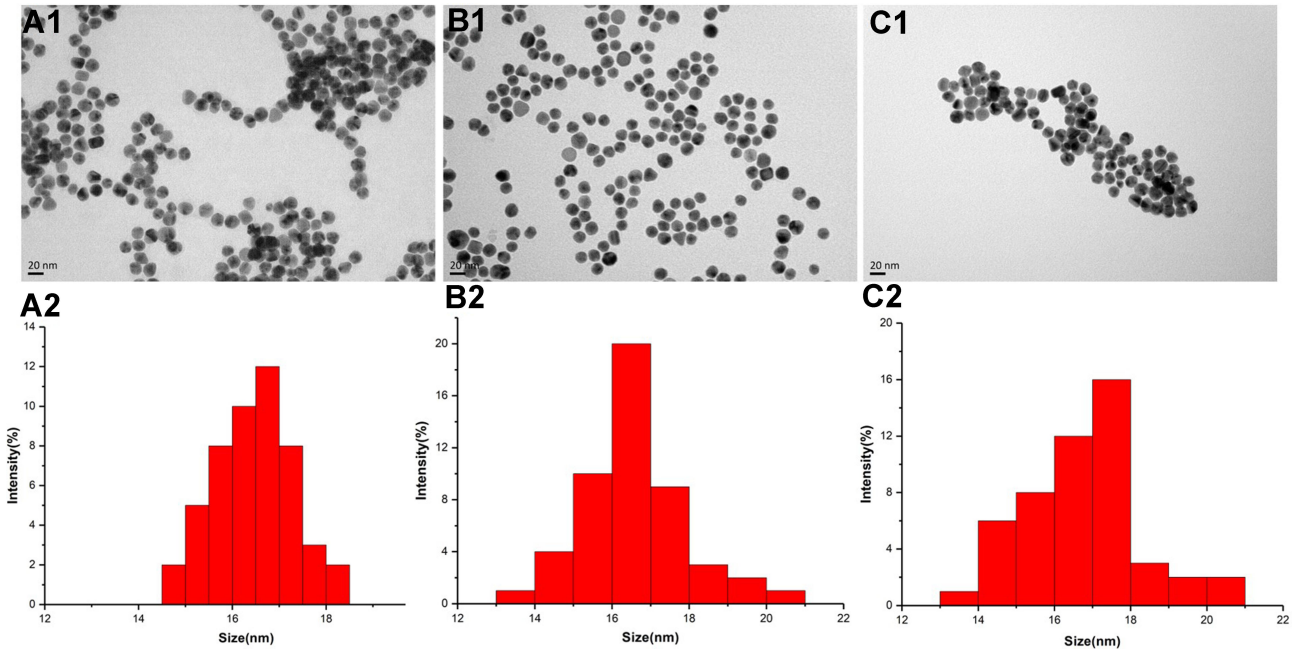

Figure 2 Transmission electron microscopic (TEM) image and size distribution of AuNPs (**A1** and **A2**), 356-AuNPs (**B1** and **B2**) and 356-TAT-AuNPs nm (**C1** and **C2**).

improve the antitumor efficacy, cell-penetrating peptide TAT was used to prepare 356-TAT-AuNPs with a diameter of 16.78 ± 1.48 nm (Figure 2C). The 356-AuNPs and 356-TAT-AuNPs are not stable at pH = 5.5 (data not shown). However, at pH = 6.5, 356-AuNPs and 356-TAT-AuNPs are stable with the average diameter of 50 nm and polydisperse index (PDI) of 0.223 measured by DLS as shown in Table S1 on the 7th day at rt. Since DLS measures the hydrated particle size, the particle size characterized by DLS is higher than the result characterized by TEM.

In vitro Antitumor Activity

To evaluate cell-penetrating peptide TAT and AuNPs that could improve the anticancer efficacy of free 356, the cell viability of HCT-116, A549 and MCF-7 cells was determined by MTT method. The result of cell viability shows that AuNPs and TAT-AuNPs exhibited no toxicity in tumor cells (Figure S2) with above 90% viability even at the high concentration of 400 μg/mL. As shown in Figure 3A–C, after being loaded with AuNPs and TAT, 356-AuNPs and 356-TAT-AuNPs exhibited low toxicity in MCF-7 and A549 cells, but decreased the viability of HCT-116 cells significantly. Moreover, 356-TAT-AuNPs induced stronger inhibition compared with free 356 and 356-AuNPs, it indicated that TAT modified gold nanoparticles could enhance free 356 antitumor activity in vitro. And the cell viability in Figure 3D shows that along with the increasing concentrations 356-TAT-AuNPs decreased the viability of HCT-116 cells significantly, while in contrast, it declined slowly on MCF-7 and A549 cells, indicating that the HCT-116 was more sensitive. On the basis of the cell viability results, HCT-116 cell line was selected for the subsequent experiments.

Apoptosis Analysis by Flow Cytometry

To explore the apoptosis inducing capability of free 356, 356-AuNPs and 356-TAT-AuNPs, the apoptosis assay was performed by FACS analysis (staining with PI and Annexin V FITC) in HCT-116 cells. As seen in Figure 4, after incubation with 5 μM free 356 for 12 h, only <10% of apoptotic cells were observed, while compared with free 356 and 356-AuNPs, 356-TAT-AuNPs induced a fairly large increase in cell apoptosis at the same concentration. After 24 h of treatment with 356-TAT-AuNPs, up to 42.3% of cancer cells underwent either

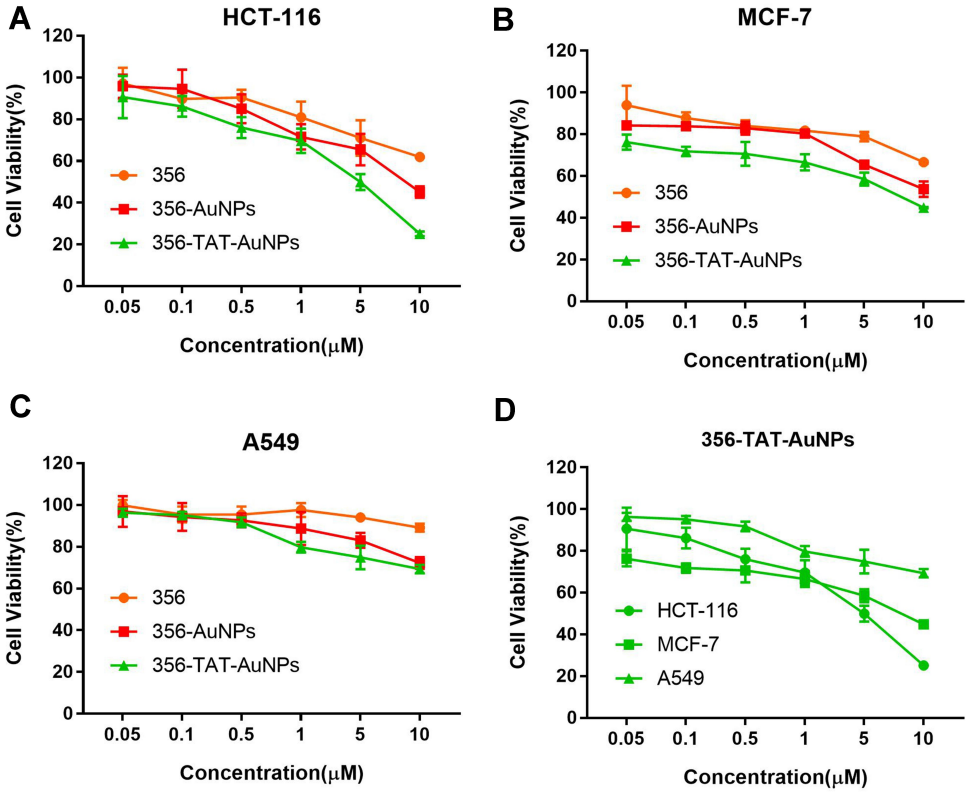

Figure 3 The in vitro cytotoxicity of free 356, 356-AuNPs and 356-TAT-AuNPs against HCT-116 (**A**), MCF-7 (**B**) and A549 (**C**) after 24h incubation, and in vitro cytotoxicity of 356-TAT-AuNPs against HCT-116, MCF-7 and A549 cells (**D**). Data represent the mean ± SD (n =6).

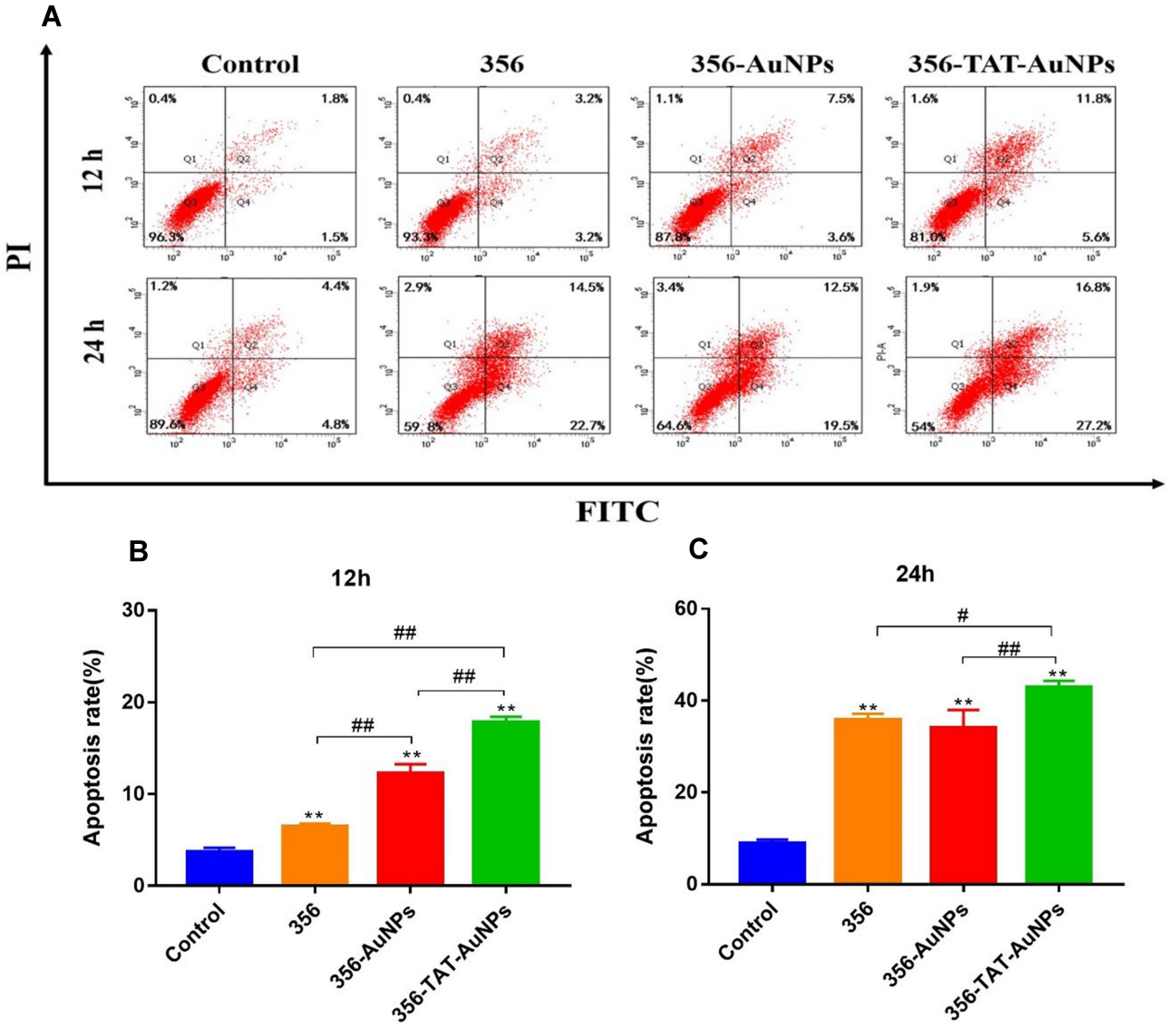

Figure 4 Effects of free 356, 356-AuNPs and 356-TAT-AuNPs to induce apoptosis of HCT-116 cells. (**A**) HCT-116 cells were treated with 5 μM compounds for 12 h and 24 h. The apoptosis rate was measured using flow cytometry. (**B**) The percentage of cells in each population for 12 h. (**C**) The percentage of cells in each population for 24 h. Data represent the mean ± SD (n =3). $^{**}p < 0.01$ vs control; $^{\#}p < 0.05$, $^{\#\#}p < 0.01$.

early apoptosis or late apoptosis. 356-TAT-AuNPs exhibited a stronger apoptotic effect than free 356 and 356-AuNPs. These results suggest that TAT modified gold nanoparticles could enhance free 356 antiapoptotic activity in vitro.

Cellular Uptake and Intracellular Distribution

In order to explore that whether TAT and AuNPs could assist in transferring free 356 into cytoplasm, the colocalization and cellular uptake of 356-TAT-AuNPs were determined using CLSM analyses using the fluorescent signal of the naphthalene group in free 356. As shown in Figure 5A, faint blue fluorescence of 356 was measured in the cells with treatment of 356, and the result implied that free 365 was not easy to penetrate through cell membranes to be taken up. However, the bright blue fluorescence was observed in 356-AuNPs and 356-TAT-AuNPs group, these figures indicated that 356-TAT-AuNPs entered HCT-116 cells effectively, and the blue fluorescence of free 356 in the 356-AuNPs and 356-TAT-AuNPs distributed all over the HCT116 cells, and primarily in the nuclei.

The cellular uptake of Au was quantified after 4 h and 24 h incubation with AuNPs, 356-AuNPs and

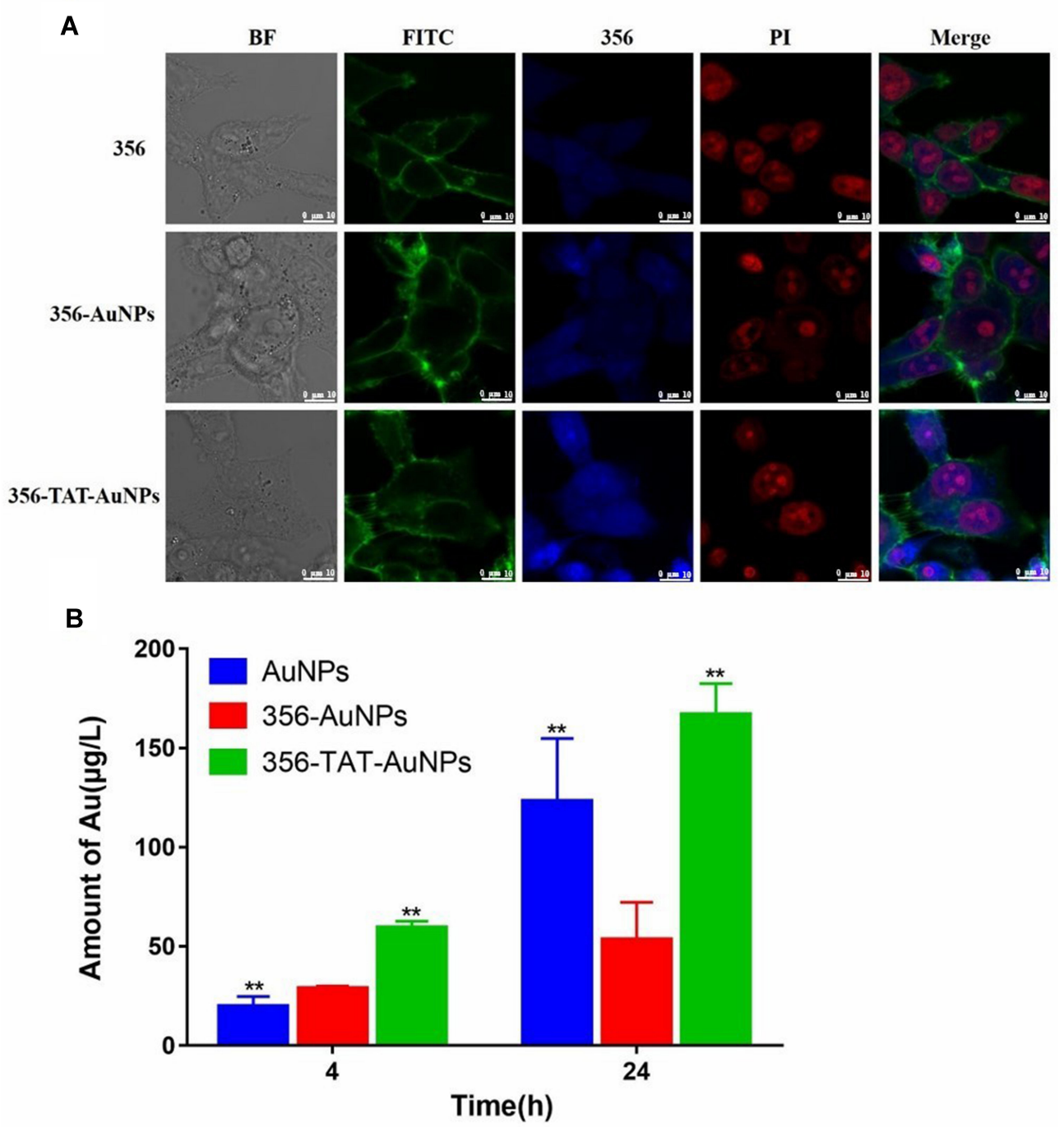

Figure 5 Cellular uptake and intracellular distribution. (**A**) Confocal laser scanning microscope images of HCT-116 cells incubated with 356 (5 μM), 356-AuNPs (5 μM), 356-TAT-AuNPs (5 μM) for 12 h. The cells were treated with PI (20 μg/mL, EM 618 nm; EX 535 nm) and FITC phalloidin (100 nM, EM 530 nm; EX 488 nm) at rt to stain the nuclei and cytoskeletons.356 was excited at the wavelength of 403 nm, and the fluorescence images were recorded at emission wavelengths of 462 nm. Scale bar: 10 μm. (**B**) The cellular uptake of AuNPs, 356-AuNPs and 356-TAT-AuNPs quantified by ICP-OES with HCT-116 cells. Data represent the mean ± SD (n =3) vs 356-AuNPs, $^{**}p < 0.01$.

356-TAT-AuNPs by ICP-OES measurement. As shown in Figure 5B, higher mass amounts of Au was taken up after incubation with 356-TAT-AuNPs compared to 356-AuNPs in 4 h. Amounts of Au showed a significant increase in uptake after 356-AuNPs treatments of 4 h and 24 h (1.9-fold). For the 356-TAT-AuNPs this resulted in a 2.8-fold higher cellular Au amount. Furthermore, amounts of Au treated with 356-TAT-AuNPs were 3.1-fold higher than the 356-AuNPs treated group after incubation with 24 h. Therefore, 356-TAT-AuNPs can penetrate into cells more efficiently. 356-TAT-AuNPs exhibited a stronger anti-cell proliferation

and apoptotic effect than 356-AuNPs, which may due to the increased uptake rate.

Inhibition of Histone H3 Citrullination

Citrullinated Histone H3 (H3Cit) is an posttranslational and irreversible modification of Arg residues in peptides or proteins, and considered a neutrophil extracellular traps (NET)-specific biomarker.[15] To further demonstrate the role of 356 in cell killing, H3Cit (Figure 6) was detected. The amount of histone H3 citrullination was analyzed using anti-histone H3 Cit 2 antibody (Abcam). The staining revealed strong nuclear labeling in the HCT-116 cell line treated with DMSO, which was less diffuse in the groups of free 356 and 356-TAT-AuNPs. Notably, 356-TAT-AuNPs was able to inhibit the H3Cit formation significantly. Meanwhile, the brighter blue fluorescence was observed in 356-TAT-AuNPs group as shown in Figure 6, which was consistent with the previous results. The results showed that free 356 can significantly increase the inhibition of H3Cit activity by means of modification with TAT and AuNPs.

AuNPs Could Enhance the 356 Releasing and Induce Autophagy in HCT-116 Cells

As showed in Figure 7A, a few nanoparticles were detected in the nucleus, mitochondria and autolysosome based on the TEM images of treating with 356-TAT-AuNPs for 24 h, perhaps suggested that peptide TAT on the surface of AuNPs facilitated either rapid escape from the endocytic system, or translocation of plasma membrane, or both. Based on the CLSM images and TEM images, the nanoparticles were distributed into cytosol and nucleus initially. After 24 h, nanoparticles become reversibly associated with endolysosomal vesicular system, especially the autolysosome, perhaps by a novel trafficking pathway.

Western Blot Analysis of Protein Expression in vitro

The formation of autophagosomes and phagophores related to the lipidation of LC3-I to yield the LC3-II protein.[16] To investigate whether 356-TAT-AuNPs treatment regulates

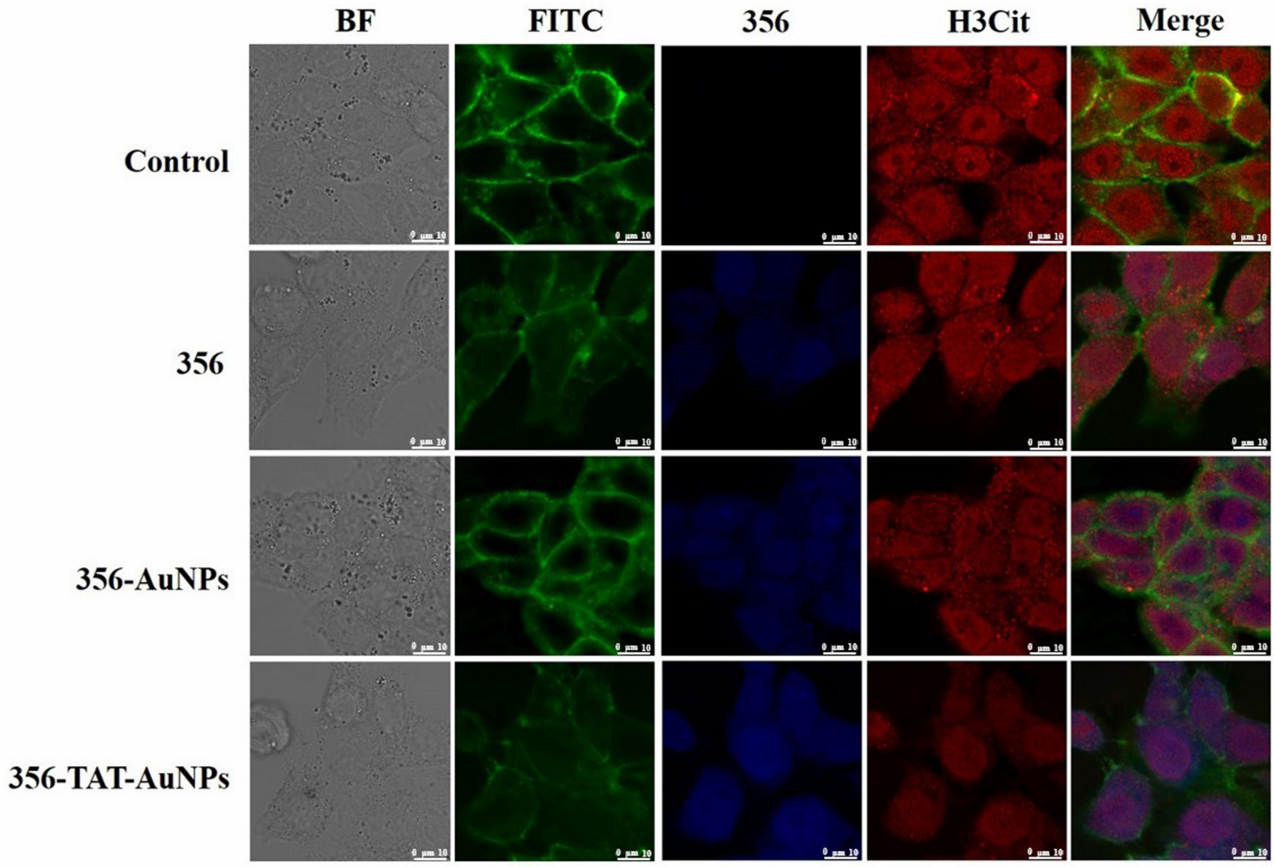

Figure 6 Confocal laser scanning microscope images of HCT-116 cells incubated with 356 (10 μM), 356-AuNPs (10 μM), 356-TAT-AuNPs (10 μM) for 12 h. The cells were treated with anti-Histone H3 antibody and FITC phalloidin (100 nM, EM 512–558 nm; EX 488 nm) to mark the Histone H3 and stain cytoskeletons.356 was excited at the wavelength of 403 nm, and the fluorescence images were recorded at emission wavelengths of 462 nm. Scale bar: 10 μm.

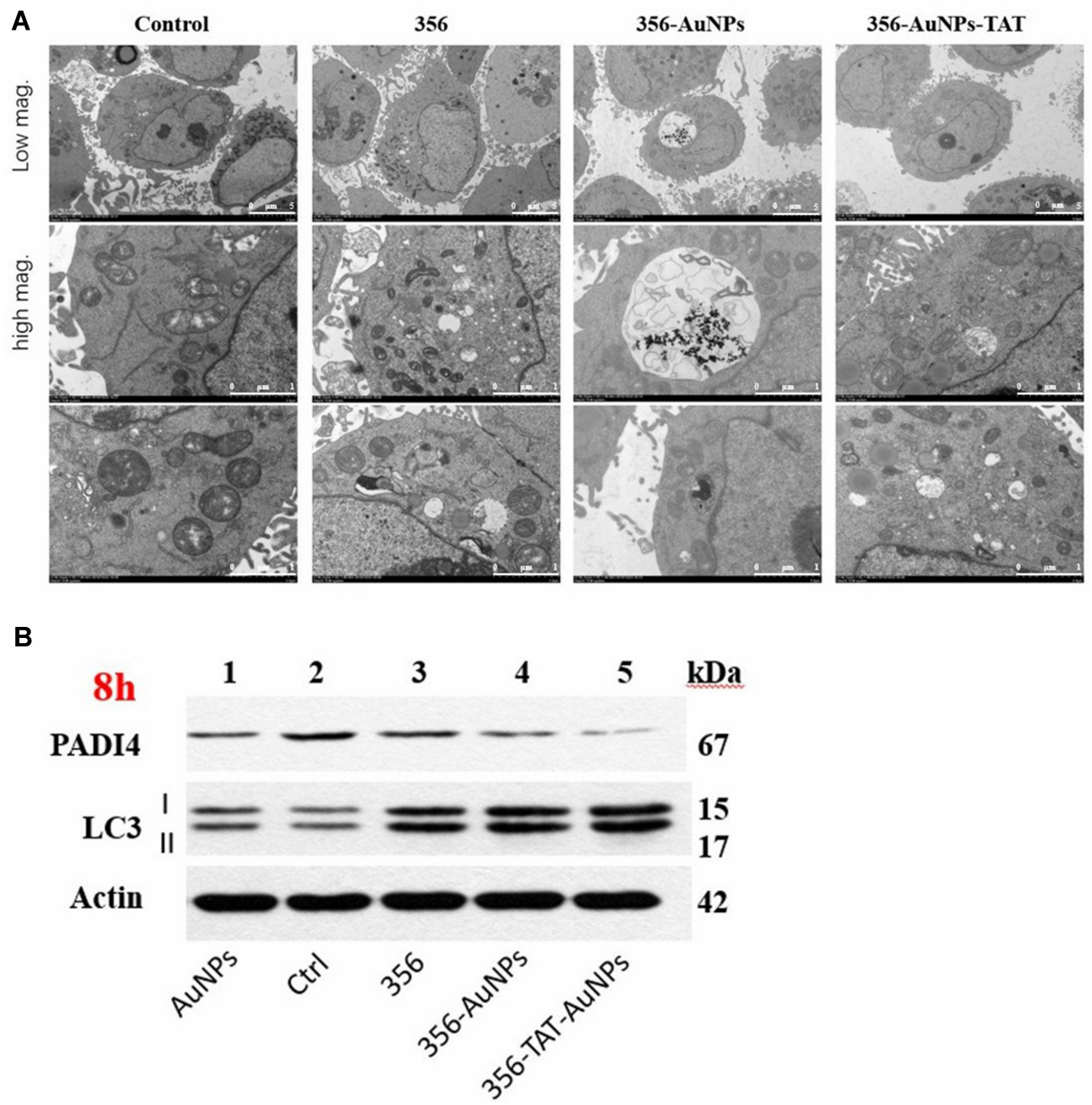

Figure 7 356-TAT-AuNPs induces autophagy in HCT-116 cells. (**A**) Transmission electron microscopy (TEM) images of HCT-116 cells treated with 356 (5 μM), 356-AuNPs (5 μM), 356-TAT-AuNPs (5 μM) for 24 h. Scale bar: 5 μm, low magnification (low mag.); 1 μm, high magnification (high mag). (**B**) Effects of AuNPs, 356, 356-AuNPs, 356-TAT-AuNPs on protein expression of HCT-116 cancer cells. Western blot analysis of proteins (PADI4 and LC3) as indicated in HCT-116 cancer cells treated with the indicated compounds for 8 h. β-actin was used as a loading control.

autophagy in HCT-116 cells, levels of LC3-II and LC3-I were analyzed by Western blotting after 356-TAT-AuNPs treatment for 8 h. LC3-II protein accumulated after 356, 356-AuNPs and 356-TAT-AuNPs treatment (Figure 7B), which is consistent with the autophagic vesicle accumulation. We found that dramatically more LC3-II accumulated in 356-TAT-AuNPs treated cells than 356 and 356-AuNPs treated cells, suggesting that 356-TAT-AuNPs inhibited autophagic vesicle breakdown by the lysosome.

As reported above, 356-TAT-AuNPs treatment decreased histone H3 citrullination by the confocal microscopy analysis (Figure 6), we further tested the levels of PAD4 by Western blotting. The results (Figure 7B) indicated that the expression of PAD4 decreased significantly

after treated with 356-TAT-AuNPs, which was consistent with the previous result.

Antitumor Efficacy in vivo

To test the effect of 356-TAT-AuNPs on tumor growth, a well-established HCT-116 cell-derived tumor bearing mice model was used.[17] After intraperitoneal injection of 356 with dose of 10 μmol/kg twice a week (BIW) for three weeks, the HCT-116 tumor growth was decreased to 51.6% comparing to the tumor size of the NS group. By conjugation to TAT and AuNPs, 356-TAT-AuNPs (1 μmol/kg) exhibited remarkable potency with a tumor growth inhibition rate of 64.1% (Figure 8C). That means, with better tumor inhibition, the concentration of 356 in 356-TAT-AuNPs group was lowed almost 10-times compared with those in 356 group. The test sample was well tolerated with no mortality and no significant body weight losses (Figure 8). Also, no significant changes in water and food. At the same time, the biodistribution study in animal model (Figure S7) was also explored, and the result had shown that AuNPs were cleared from the bloodstream rapidly by i.v. by the reticuloendothelial system, and mainly accumulated in the tumor, spleen and liver.

Discussion and Conclusion

Recently, the development of AuNPs for the antitumor agent delivery has drawn lots of attention from the medical and drug research community. AuNPs (size 20 nm) have been modified with varied targeting peptides for functionalizing nanoparticles with biological membranes penetrating and nucleus targeting effects.[18] CPPs have drawn great attention due to their special ability to regulate uptake of different cargos such as drugs, DNA, and siRNA.[19–21] The PAD4 is overexpressed in a majority of human cancers markedly, indicating that PAD4 could be a putative target in cancer treatment. Compound 356, a PAD4 inhibitor, activates *p53* target genes to inhibit cancer growth,[7,22,23] but the water solubility of 356 is rather poor.

For successful chemotherapy, highly efficient targeted drug delivery is crucial. In this study, TAT-AuNPs were developed as the drug delivery system which could load anticancer compoud 356 via interaction with AuNPs modified by peptide TAT. 356-TAT-AuNPs suppressed the growth of HCT-116, MCF-7 and A549 cells significantly, among them the cell line HCT-116 was more sensitive to 356-TAT-AuNPs. Yuzhalin et al reported that the Cit of the extracellular matrix (ECM) molecules catalyzing by extracellular PAD4 was an key event in changing colorectal cancer cell signaling.[6] Unlike the colorectal tumor cells, downregulation of PAD4 expression in breast tumor cells led to increase of epithelial-to-mesenchymal transition markers (Smad4 and p-Smad2),[24] while the overexpression of PAD4 in lung tumor cells inhibited epithelial-to-mesenchymal transition through suppression of Elk1.[25] The release of PAD4 of tumor cells is obviously complex. PAD4 inhibitors may act on tumor cells through different signals, which may be the reason for the relative sensitivity to HCT-116. Besides, TAT-AuNPs was used to improve the cellular uptake. The experimental results showed that TAT-AuNPs provided excellent efficacy in delivering 356 into HCT-116 cells. To explore the targeting effect into HCT-116 cells, the HCT-116 xenografted mice model was used. And the result of this in vivo bioassay showed that the tumor inhibition rate of the treatment of 356-TAT-AuNPs was the highest among all the groups.

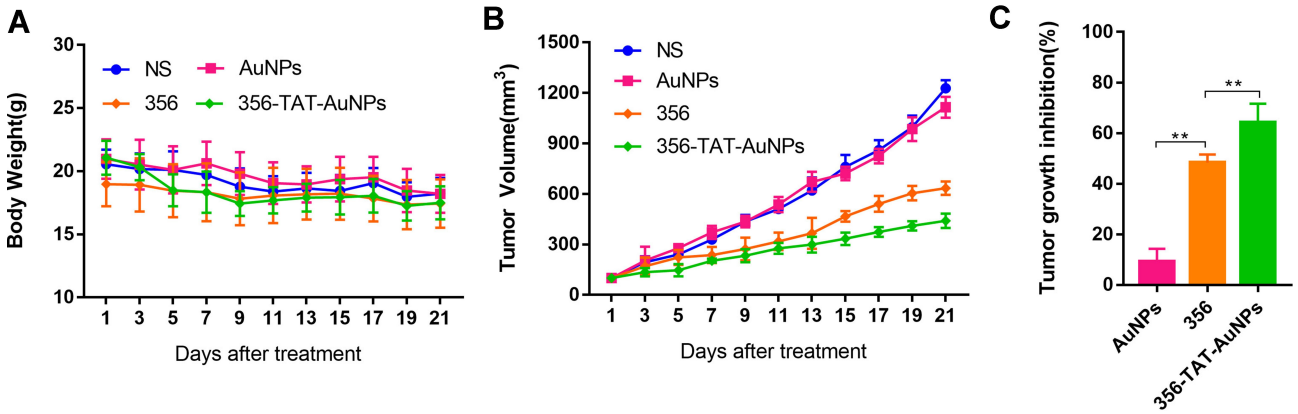

Figure 8 Effects of AuNPs, 356 and 356-TAT-AuNPs treatment on the tumorigenicity of HCT-116 cells in vivo. (**A**) The nude mouse body weight was measured every 2 days. (**B**) The tumor volumes of the nude mice were measured and calculated once every 2 days. (**C**) tumor growth inhibition from tumor-bearing mice after received different treatments on the 21st day. Data represent the mean ± SD (n =5). $^{**}p < 0.01$.

In this work, an effective drug delivery system on the basis of peptide TAT modified AuNPs loading PAD4 inhibitor 356 was designed, prepared, and applied to augment the anticancer efficacy. This work proved that the 356-TAT -AuNPs exhibited about 16.7 nm nano-sized characteristics, improved the activity in cell membrane penetration and PAD4 inhibition with a clearly increase in cell uptake and induced tumor cell death, thereby, leading to killing tumor cells with higher efficacy. The antitumor results in vivo indicated that the combination of peptide TAT and AuNPs as drug carrier is potent in inhibiting tumor growth and could be a powerful strategy for improved development of anticancer drug. Taken together, our study demonstrates the design of new PAD4 inhibitor-nano delivery system TAT-AuNPs exhibited higher efficient drug release and tumor specificity. So the precisely designed and prepared nanostructure showed a synergistic efficacy for the antitumor drug and thus may solve the current problems of using nanosystems in systematic administration.

Acknowledgments

This study was supported by the Beijing Municipal Colleges and Universities High Level Talents Introduction and Cultivate Project-Beijing Great Wall Scholar program (CIT&TCD 20180332), Scientific Research Common Program of Beijing Municipal Commission of Education (KM201810025011), and Scientific research and Cultivation Fund of Capital Medical University (PYZ19145).

Disclosure

The authors report no conflicts of interest in this work.

References

1. Curran AM, Naik P, Giles JT, Darrah E. PAD enzymes in rheumatoid arthritis: pathogenic effectors and autoimmune targets. *Nat Rev Rheumatol*. 2020;16:301–315. doi:10.1038/s41584-020-0409-1
2. Vossenaar ER, Zendman AJ, van Venrooij WJ, Pruijn GJ. PAD, a growing family of citrullinating enzymes: genes, features and involvement in disease. *Bioessays*. 2003;25(11):1106–1118. doi:10.1002/bies.10357
3. Anzilotti C, Pratesi F, Tommasi C, Migliorini P. Peptidylarginine deiminase 4 and citrullination in health and disease. *Autoimmun Rev*. 2010;9(3):158-160. doi:10.1016/j.autrev.2009.06.002
4. Darrah E, Andrade F. Rheumatoid arthritis and citrullination. *Curr Opin Rheumatol*. 2018;30(1):72–78. doi:10.1097/BOR.0000000000000452
5. Wang Y, Li M, Stadler S, et al. Histone hypercitrullination mediates chromatin decondensation and neutrophil extracellular trap formation. *J Cell Biol*. 2009;184(2):205-213. doi:10.1083/jcb.200806072
6. Yuzhalin AE, Gordon-Weeks AN, Tognoli ML, et al. Colorectal cancer liver metastatic growth depends on PAD4-driven citrullination of the extracellular matrix. *Nat Commun*. 2018;9(1):4783. doi:10.1038/s41467-018-07306-7
7. Wang Y, Li P, Wang S, et al. Anticancer peptidylarginine deiminase (PAD) inhibitors regulate the autophagy flux and the mammalian target of rapamycin complex 1 activity. *J Biol Chem*. 2012;287(31):25941–25953. doi:10.1074/jbc.M112.375725
8. Jahangirian H, Kalantari K, Izadiyan Z, Rafiee-Moghaddam R, Shameli K, Webster TJ. A review of small molecules and drug delivery applications using gold and iron nanoparticles. *Int J Nanomedicine*. 2019;14:1633–1657. doi:10.2147/IJN.S184723
9. Darabdhara G, Das MR, Singh SP, Rengan AK, Szunerits S, Boukherroub R. Ag and Au nanoparticles/reduced graphene oxide composite materials: synthesis and application in diagnostics and therapeutics. *Adv Colloid Interface Sci*. 2019;271:101991. doi:10.1016/j.cis.2019.101991
10. Connor DM, Broome AM. Gold nanoparticles for the delivery of cancer therapeutics. *Adv Cancer Res*. 2018;139:163–184. doi:10.1016/bs.acr.2018.05.001
11. Torchilin VP, Levchenko TS, Rammohan R, Volodina N, Papahadjopoulos-Sternberg B, D'Souza GG. Cell transfection *in vitro* and *in vivo* with nontoxic TAT peptide-liposome-DNA complexes. *Proc Natl Acad Sci U S A*. 2003;100(4):1972-1977. doi:10.1073/pnas.0435906100
12. Torchilin VP. Tat peptide-mediated intracellular delivery of pharmaceutical nanocarriers. *Adv Drug Deliv Rev*. 2008;60(4–5):548–558. doi:10.1016/j.addr.2007.10.008
13. Duan Z, Chen C, Qin J, et al. Cell-penetrating peptide conjugates to enhance the antitumor effect of paclitaxel on drug-resistant lung cancer. *Drug Deliv*. 2017;24(1):752–764. doi:10.1080/10717544.2017.1321060
14. Wu J, Gao W, Yang H, Zuo JM. Dissolution kinetics of oxidative etching of cubic and icosahedral platinum nanoparticles revealed by in situ liquid transmission electron microscopy. *ACS Nano*. 2017;11(2):1696-1703. doi:10.1021/acsnano.6b07541
15. Konig MF, Andrade F. A critical reappraisal of neutrophil extracellular traps and NETosis mimics based on differential requirements for protein citrullination. *Front Immunol*. 2016;7:461. doi:10.3389/fimmu.2016.00461
16. Rinchai D, Riyapa D, Buddhisa S, et al. Macroautophagy is essential for killing of intracellular Burkholderia pseudomallei in human neutrophils. *Autophagy*. 2015;11(5):748-755. doi:10.1080/15548627.2015.1040969
17. Fluckiger A, Dumont A, Derangère V, et al. Inhibition of colon cancer growth by docosahexaenoic acid involves autocrine production of TNFα. *Oncogene*. 2016;35(35):4611-4622. doi:10.1038/onc.2015.523
18. Daraee H, Eatemadi A, Abbasi E, Fekri Aval S, Kouhi M, Akbarzadeh A. Application of gold nanoparticles in biomedical and drug delivery. *Artif Cells Nanomed Biotechnol*. 2016;44(1):410-422. doi:10.3109/21691401.2014.955107
19. Loh XJ, Lee TC, Dou Q, Deen GR. Utilising inorganic nanocarriers for gene delivery. *Biomater Sci*. 2016;4(1):70-86. doi:10.1039/c5bm00277j
20. Farkhani SM, Valizadeh A, Karami H, Mohammadi S, Sohrabi N, Badrzadeh F. Cell penetrating peptides: efficient vectors for delivery of nanoparticles, nanocarriers, therapeutic and diagnostic molecules. *Peptides*. 2014;57:78-94. doi:10.1016/j.peptides.2014.04.015
21. Wang Z, Liu G, Zheng H, Chen X. Rigid nanoparticle-based delivery of anti-cancer siRNA: challenges and opportunities. *Biotechnol Adv*. 2014;32(4):831-843. doi:10.1016/j.biotechadv.2013.08.020
22. Wang S, Chen XA, Hu J, et al. ATF4 gene network mediates cellular response to the anticancer PAD inhibitor YW3-56 in triple-negative breast cancer cells. *Mol Cancer Ther*. 2015;14(4):877–888. doi:10.1158/1535-7163.MCT-14-1093-T

23. Liang Y, Pan B, Alam HB, et al. Inhibition of peptidylarginine deiminase alleviates LPS-induced pulmonary dysfunction and improves survival in a mouse model of lethal endotoxemia. *Eur J Pharmacol*. 2018;833:432-440. doi:10.1016/j.ejphar.2018.07.005
24. Stadler SC, Vincent CT, Fedorov VD, et al. Dysregulation of PAD4-mediated citrullination of nuclear GSK3β activates TGF-β signaling and induces epithelial-to-mesenchymal transition in breast cancer cells. *Proc Natl Acad Sci U S A*. 2013;110(29):11851-11856. doi:10.1073/pnas.1308362110
25. Duan Q, Pang C, Chang N, Zhang J, Liu W. Overexpression of PAD4 suppresses drug resistance of NSCLC cell lines to gefitinib through inhibiting Elk1-mediated epithelial-mesenchymal transition. *Oncol Rep*. 2016;36(1):551–558. doi:10.3892/or.2016.4780